Available online at www.sciencedirect.com
SCIENCE DIRECT®
Journal of Power Sources 144 (2005) 191–196
JOURNAL OF POWER SOURCES
www.elsevier.com/locate/jpowsour

Hydrophobic ionic liquids based on the 1-butyl-3-methylimidazolium cation for lithium/seawater batteries

Yancheng Zhang [a, 1], Mirna Urquidi-Macdonald [b, *, 2]

[a] *Center for Electrochemical Science and Technology, Pennsylvania State University, University Park, PA 16802, USA*
[b] *Department of Engineering Science and Mechanics, Pennsylvania State University, University Park, PA 16802, USA*

Received 16 November 2004; received in revised form 20 December 2004; accepted 20 December 2004
Available online 9 March 2005

Abstract

Two hydrophobic ionic liquids (room temperature molten salts) based on 1-butyl-3-methylimidazolium cation (BMI^+), $BMI^+PF_6^-$ and $BMI^+Tf_2N^-$, were used in developing a highly efficient lithium anode system for lithium/seawater batteries. The lithium anode system was composed of lithium metal/ionic liquid/Celgard membrane. Both $BMI^+PF_6^-$and $BMI^+Tf_2N^-$ maintained high apparent anodic efficiency (up to 100%) under potentiostatic polarization (at +0.5 V versus open-circuit potential (OCP)) in a 3% NaCl solution. Eventually, traces of water contaminated the ionic liquid and a bilayer film (LiH and LiOH) on the lithium surface was formed, decreasing the rate of lithium anodic reaction and hence the discharge current density. $BMI^+Tf_2N^-$ prevented traces of water from reaching the lithium metal surface longer than $BMI^+PF_6^-$ (60 h versus 7 h). However, $BMI^+PF_6^-$ was better than $BMI^+Tf_2N^-$ in keeping a constant current density ($\sim$0.2 mA cm^{-2}) before the traces of water contaminated the lithium surface due to the non-reactivity of $BMI^+PF_6^-$ with the lithium metal that kept the bare lithium surface. During the discharge process, $BMI^+PF_6^-$ and $BMI^+Tf_2N^-$ acted as ion transport media of Li^+, Cl^-, OH^- and H_2O, but did not react with them because of the excellent chemical stability, high conductivity, and high hydrophobicity of these two ionic liquids. Both $BMI^+PF_6^-$ and $BMI^+Tf_2N^-$ gels were tentative approaches used to delay the traces of water coming in contact with the lithium surface.

Keywords: 1-Butyl-3-methyl-imidazolium hexafluorophosphate ($BMI^+PF_6^-$); 1-Butyl-3-methyl-imidazolium bis((trifluoromethyl)sulfonyl)amide ($BMI^+Tf_2N^-$); Hydrophobic ionic liquid; Room temperature molten salt; Lithium/seawater battery

1. Introduction

The electrochemical application of ionic liquids (room temperature molten salts) that exhibit attractive properties such as high ionic conductivity ($\sim 10^{-3}$ S cm^{-1}), wide electrochemical window (more than 3.0 V), and excellent thermal and chemical stability, has been explored in the fields of photoelectrochemical (solar) cells [1,2], lithium secondary batteries [3–5] and electrochemical capacitors [6]. Dialkylimidazolium based ionic liquids with the weakly complexing anions (e.g. PF_6^-, BF_4^-, or $CF_3SO_3^-$, $(CF_3SO_2)_2N^-$) seem to be the most stable and conductive to date [7–10]. The 1-butyl-3-methylimidazole (BMI^+)-based ionic liquids with PF_6^- [5] and $(CF_3SO_2)_2N^-$ (abbr. Tf_2N^-) [9] have high hydrophobicity besides other good properties (Table 1) [5,8,9,11].

The high reactivity of lithium with water results in low efficiency of lithium-seawater batteries [12–15]. In this paper, two hydrophobic ionic liquids ($BMI^+PF_6^-$ and $BMI^+Tf_2N^-$) are used to separate the water from the lithium surface in order to develop a highly efficient lithium anode system for lithium/seawater batteries. A Celgard® 3400 microporous membrane (Celgard Inc.), 25 μm thick and with low electric resistivity (0.04 Ω cm^2), [16] is used to keep the ionic liquids in place. The tiny pores (0.117 μm × 0.042 μm [16]) enable it to operate as a good water and gas barrier.

* Corresponding author. Tel.: +1 814 863 4217; fax: +1 814 863 7967.
E-mail address: mumesm@engr.psu.edu (M. Urquidi-Macdonald).
[1] Electrochemical Society Student Member.
[2] Electrochemical Society Active Member.

0378-7753/$ – see front matter © 2005 Elsevier B.V. All rights reserved.
doi:10.1016/j.jpowsour.2004.12.050

Table 1
The main properties of $BMI^+PF_6^-$ and $BMI^+Tf_2N^-$

Ionic liquid	Melting point (°C)	Water saturation content (mass%)	Dynamic viscosity (cP)	Conductivity (mS cm^{-1})	Density (g cm^{-3})
$BMI^+PF_6^-$	−61 [8]	4 at 25 °C [11]	312 at 30 °C [8]	1.8 at 22 °C [5]	1.37 at 30 °C [8]
$BMI^+Tf_2N^-$	−4 [9]	1.4 at 20 °C [9]	52 at 20 °C [9]	3.9 at 20 °C [9]	1.429 at 19 °C [9]

2. Experimental

2.1. Chemicals and synthesis

Bromobutane (Aldrich, 99.0%) and 1-methylimidazole (Aldrich, 99%) were mixed in 1,1,1-trichloroethane (Aldrich, 99.5%) and refluxed to get yellowish 1-butyl-3-methylimidazolium bromide (BMI^+Br^-). $BMI^+PF_6^-$ or $BMI^+Tf_2N^-$ was synthesized with BMI^+Br^- and KPF_6 (Aldrich, 98%) or $LiTf_2N$ (Aldrich, 99.0%) by the following metathesis reactions,

$$BMI^+Br^- + KPF_6 \rightarrow BMI^+PF_6^- \quad (1)$$

$$BMI^+Br^- + LiTf_2N \rightarrow BMI^+Tf_2N^- \quad (2)$$

The syntheses of the ionic liquids [9,11,17] was very important to assure their purity and high hydrophobicity.

2.2. Electrochemical cell and instrumentation

The lithium anode system (lithium/ionic liquid/Celgard), in the glove box under argon atmosphere, was set into an anode holder especially designed to avoid water leakage (Fig. 1). The anode system was "activated" by submerging it in a 3% NaCl solution after being moved outside the glove box. A buret with an inverted funnel was placed above the lithium anode system to collect hydrogen gas. A nickel wire was used outside of the funnel as the cathode (Fig. 1). The lithium surface area exposed to the ionic liquid (2.5 cm thick) and the area of Celgard membrane exposed to the 3% NaCl solution were always equal to 0.71 cm^2. A Solatron SI 1280B Electrochemical Measurement System was used for the potentiostatic polarization experiments and electrochemical impedance spectroscopy (EIS) measurement.

3. Results and discussion

3.1. Lithium/$BMI^+PF_6^-$ interface and lithium/$BMI^+Tf_2N^-$ interface

The lithium anodic reaction on the lithium metal is indicative of the performance of the lithium anode system. The interfacial property of the lithium surface in contact with $BMI^+PF_6^-$ or $BMI^+Tf_2N^-$ is vitally important for the electrochemical reaction on the lithium surface in the lithium/ionic liquid/Celgard anode system.

The lithium/$BMI^+PF_6^-$ interface remained metallic and "silvery" looking on the surface (to the naked eye) after 12 h in the glove box. A SEM image of this interface (after vacuum removing any liquid $BMI^+PF_6^-$) is shown in Fig. 2(a). Comparably, it has a similar pattern to that in the SEM image of $BMI^+PF_6^-$ on a platinum surface (after vacuum removing any liquid $BMI^+PF_6^-$), shown in Fig. 2(b). The former patterns look more separated, probably because of the formation of LiOH resulting from traces of water contaminating the sample (water coming from the air humidity when the sample was moved outside of the glove box to the SEM). The image similarity shows the non-reactivity of $BMI^+PF_6^-$ with

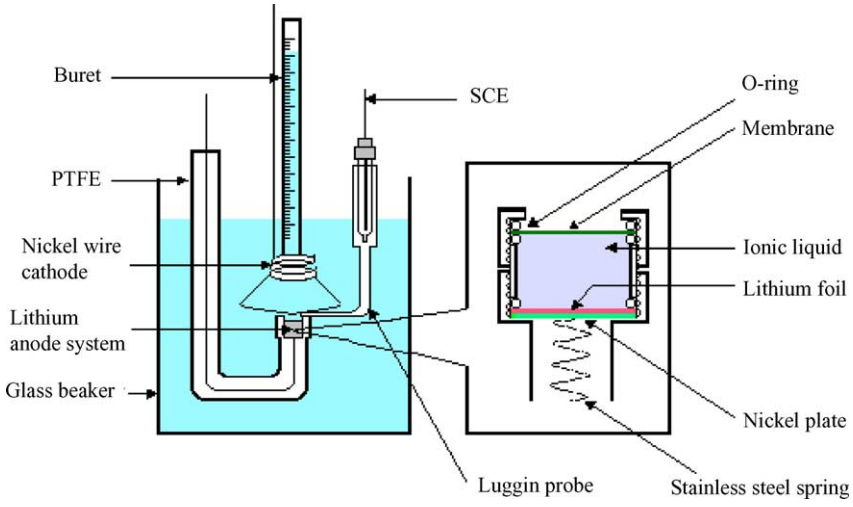

Fig. 1. Electrochemical measurement setup for lithium/ionic liquid/Celgard anode system.

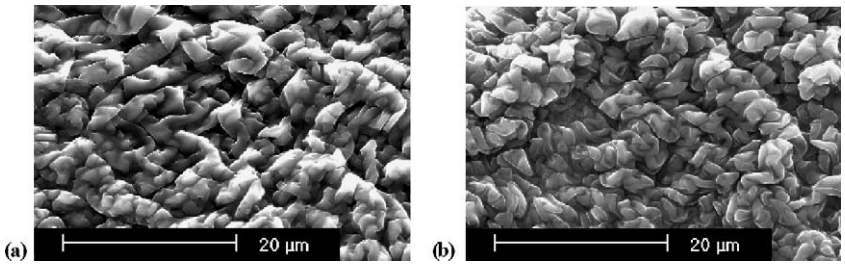

Fig. 2. (a) SEM image of a "silvery" looking lithium surface with $BMI^+PF_6^-$; (b) SEM image of $BMI^+PF_6^-$ on a platinum surface (after vacuum removing any liquid $BMI^+PF_6^-$).

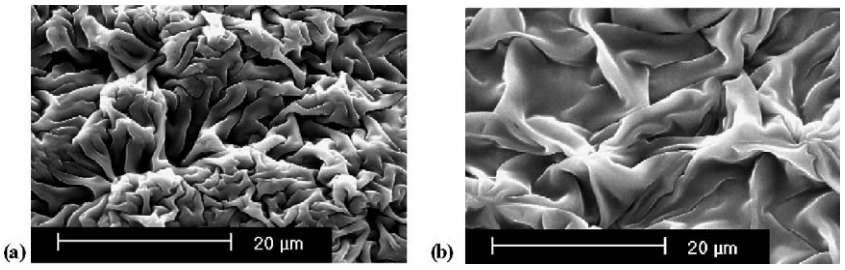

Fig. 3. (a) SEM image of black lithium surface with $BMI^+Tf_2N^-$; (b) SEM image of $BMI^+Tf_2N^-$ on a platinum surface (after vacuum removing any liquid $BMI^+Tf_2N^-$).

lithium, similar to the non-reactivity of $BMI^+PF_6^-$ with the platinum surface, which is noble.

The lithium/$BMI^+Tf_2N^-$ interface produced a black film on the lithium over a period of 12 h. SEM images show the different patterns for the black film on the lithium surface and $BMI^+Tf_2N^-$ film on a platinum surface (Fig. 3(a) and (b)). The former looks thicker and more porous. Its composition was not investigated, but from its color and nature it is anticipated to include brown lithium nitride Li_3N since [18,19] proposed that it is possible to produce Li_3N via reduction reaction of Tf_2N^- with lithium metal. The black film on the lithium–$BMI^+Tf_2N^-$ interface impacted the electrochemical behavior of the lithium anode system in seawater.

3.2. *Lithium anode system respectively with $BMI^+PF_6^-$ and $BMI^+Tf_2N^-$ in seawater*

Water contamination changes the lithium/ionic liquid interfacial properties. The interfacial change may be reflected in the measured discharge current density with time for the potentiostatic polarization (+0.5 V versus OCP) of the lithium anode system (respectively with $BMI^+PF_6^-$ or $BMI^+Tf_2N^-$) in seawater (Fig. 4). The measured OCP of the lithium anode systems used in this work was in the range of −2.65 V to −2.90 V versus saturated calomel electrode (SCE).

The lithium anode system with $BMI^+PF_6^-$ initially exhibited a constant polarization current density at ∼0.2 mA cm^{-2} for around 7 h. Thereafter, a sharp inflexion was seen in the curve of the current density with time. This quick decrease of current density resulted from the bilayer film (LiH and LiOH) formed due to trace water penetration through $BMI^+PF_6^-$ and onto the lithium surface [11]. The almost constant current density before the trace water contamination and the sensitive response of lithium–$BMI^+PF_6^-$interface to trace water contamination together illustrate an existing "fresh and active" lithium surface due to the non-reactivity of $BMI^+PF_6^-$ with lithium. Before trace water contamination with the lithium surface, lithium dissolution reaction ($Li \rightarrow Li^+ + e$) took place on the stable lithium/$BMI^+PF_6^-$ interface, and Li^+ ions transported through $BMI^+PF_6^-$ and into the 3% NaCl solution under the action of electromigration and diffusion. At the same time, OH^- ions, produced on the cathode ($O_2 + 2H_2O + 4e \rightarrow 4OH^-$ and $H_2O + e \rightarrow \frac{1}{2}H_2 + OH^-$), transported in the reverse direction with much lower diffusion flux (than Li^+ ions) due to much lower concentration gradient following the dilution of OH^- ions in the 3% NaCl solution. Water molecule and Cl^- ions also moved to the anode through $BMI^+PF_6^-$. When water molecule reached the lithium sur-

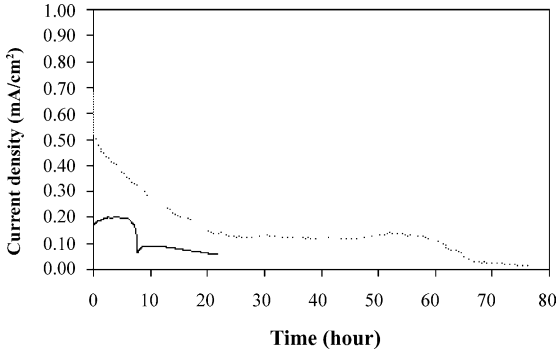

Fig. 4. Current density of lithium/ionic liquid/Celgard anode systems at the potentiostatic polarization of +0.5 V (vs. OCP): (—) $BMI^+PF_6^-$; (···) $BMI^+Tf_2N^-$.

face, trace water contamination happened and decreased the rate of lithium dissolution reaction, which was discussed in [11]. It is important to note that $BMI^+PF_6^-$, prepared from imidazolium halide (including chloride) and $LiPF_6$ in aqueous solution [7–9], is stable to Li^+, Cl^- and H_2O. And low concentration of OH^- after its dilution in the 3% NaCl solution is unlikely to dissolve $BMI^+PF_6^-$. Accordingly, $BMI^+PF_6^-$ only acted as transport media of Li^+, Cl^-, OH^- and H_2O. No reaction occurred and only ionic transport process happened at the interface of $BMI^+PF_6^-$/Celgard/water.

For the lithium anode system with $BMI^+Tf_2N^-$, the current density continuously decreased from 0.52 mA cm^{-2} to 0.12 mA cm^{-2} during the 24 h of polarization at +0.5 V (versus OCP) and remained constant at 0.12 mA cm^{-2} until the sixtieth hour of the polarization. Then, a slow inflexion existed for the current density with time, though not as sharp as that of the lithium anode system with $BMI^+PF_6^-$, because the lithium–$BMI^+Tf_2N^-$ interfacial film appears to moderate the lithium–water reaction and slow the formation of the bilayer film (LiH and LiOH). The gradually diminishing current density over the initial 24 h of the polarization corresponds to the forming and progressive filling of the porous film at the lithium–$BMI^+Tf_2N^-$ interface followed by decreasing the rate of lithium dissolution reaction [20,21]. Since $BMI^+Tf_2N^-$ is more hydrophobic than $BMI^+PF_6^-$, it took longer (60 h versus 7 h) to display the trace water contamination shown by the inflexion. Notablely, like $BMI^+PF_6^-$, $BMI^+Tf_2N^-$ also acted as transport media of Li^+, Cl^-, OH^- and H_2O, but did not react with them on account of its excellent chemical stability, high conductivity and high hydrophobicity (Table 1) [7–9].

Both the lithium anode systems with $BMI^+PF_6^-$ and $BMI^+Tf_2N^-$ kept apparent anodic efficiency up to 100% since no hydrogen gas was found in the anode system or trapped under the Celgard membrane during the whole period of the potentiostatic polarization. The results showed that both hydrophobic ionic liquids ($BMI^+PF_6^-$ and $BMI^+Tf_2N^-$) were able to stop the production of hydrogen gas from contact with the lithium surface. Trace water penetration decreased current density, but did not drop the apparent anodic efficiency considerably [11].

3.3. Lithium anode system with hydrophobic silica-gel

Hydrophobic silica-gel was used in an attempt to delay or avoid traces of water penetrating into the ionic liquid and reaching the lithium surface. Amorphous fumed silica (CAB-O-SIL® TS-530, average particle length 0.2 μm–0.3 μm, Cabot Corporation) is considered "high-purity" silica treated with hexamethyldisilazane to be extremely hydrophobic. When it is mixed together with the ionic liquid and polyethyleneoxide (PEO, average $M_v \sim 4{,}000{,}000$, Aldrich), hydrophobic silica-gel is formed with higher hydrophobicity than the corresponding ionic liquid. PEO is employed as a surfactant to ensure proper mixing of the silica and the ionic liquid. Thorough mixing and uniform blending are very important to obtain uniform gel and to prevent the formation of silica lumps in the gel. The mixing weight ratios of the three kinds of hydrophobic silica-gels (Table 2) were attempted in the lithium anode system schematically shown in Fig. 5. $BMI^+PF_6^-$ (3 mm thick) was sandwiched between lithium and the hydrophobic silica-gel due to the active lithium surface with $BMI^+PF_6^-$ and lower contact resistance with lithium than direct contact of gel with lithium.

Table 2
Weight ratios of three kinds of hydrophobic silica-gels

Gel no.	Ionic liquid	Silica (wt.%)	PEO (wt.%)
1	$BMI^+PF_6^-$	1	2
2	$BMI^+PF_6^-$	1.5	3
3	$BMI^+Tf_2N^-$	1.5	3

Note: wt.% of silica or PEO represents weight percent with respect to $BMI^+PF_6^-$ or $BMI^+Tf_2N^-$.

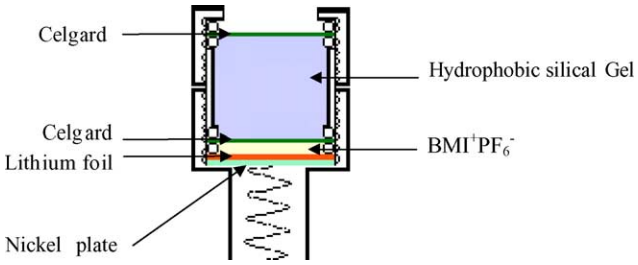

Fig. 5. Schematic of a lithium anode system with hydrophobic silica-gel (lithium/$BMI^+PF_6^-$/Celgard/hydrophobic silica-gel/Celgard).

The electrochemical impedance spectroscopy of the lithium anodes with different gels was measured with an AC potential 10 mV (peak to peak) at open-circuit potential (OCP) and sweep frequency ranged from 20 kHz to 0.01 Hz (Fig. 6). Solution resistance (including gel resistance), R_S, is obtained from high-frequency impedance and displays a higher conductivity of $BMI^+Tf_2N^-$ gel than BMI^+PF_6 gel. The depressed semicircle (around 80 Hz) is a strong indication of a system with lithium surface roughness and the tortuous path of Li^+ throughout the ionic liquid at the lithium/ionic liquid interface [11,22–25]. The charge transfer resistance (R_P) estimated from the diameter of the semicircle and the frequency f_{max} (the frequency corresponding to the maximum imaginary component in the semicircle) are close for three lithium anode systems respectively with three kinds of silica-gels (Fig. 6 and Table 3). Corresponding to the semicircles, the time constants $\tau = 1/(2\pi f_{max})$ are also close (2.0 ms–2.5 ms), which represent, to a great extent, the sim-

Table 3
A comparison of parameter values from electrochemical impedance spectra in Fig. 6

Parameter	R_S (Ω)	R_P (Ω)	f_{max} (Hz)	Time constant, τ (ms)	Slope angle, θ (°)
Gel 1	2280	1250	80	2.0	−6
Gel 2	2490	780	80	2.0	−6
Gel 3	1280	780	63	2.5	−10

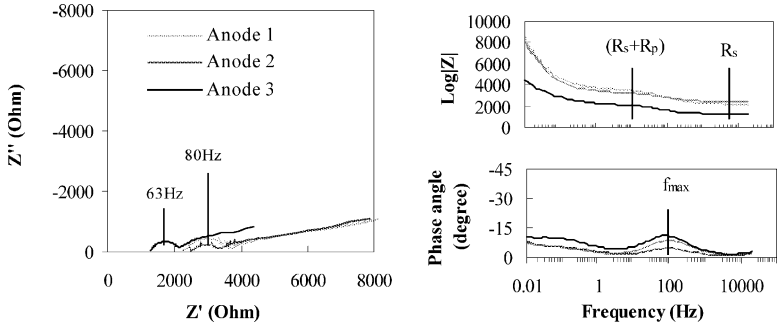

Fig. 6. Electrochemical impedance spectra of three lithium anode systems respectively with different silica-gels. *Note*: Anode 1, 2, 3 in the figure respectively represent three lithium anode systems (lithium/BMI$^+$PF$_6$$^-$/Celgard/gel/Celgard) with different gel 1, 2, 3. The ratios of gel 1, 2 and 3 are listed in Table 2.

ilar interfacial properties of lithium/BMI$^+$PF$_6$$^-$, in the three lithium anode systems. At low frequencies, the straight tails with low slopes (around 10°) are related to the ion diffusion process of the electroactive species. Such low slopes, much deviated from 45° slope for a normal diffusion impedance, result from the limited dimensionality of the diffusion path (of the electroactive species) imposed by the gel porosity due to the dispersion effects from the silica-gel [25,26]. Comparably, the impedance for the lithium/ionic liquid system without gel had a diffusion impedance with 45° slope [11]. Among the three slopes, a little higher slope (or less deviation from 45°) exists with BMI$^+$Tf$_2$N$^-$ gel because BMI$^+$Tf$_2$N$^-$ has a lower dynamic viscosity than BMI$^+$PF$_6$$^-$ (Table 1) permits to possess less porosity.

The lithium anode system with BMI$^+$PF$_6$$^-$ gel outputted constant current density at ~0.1 mA cm^{-2} for 30 h (gel 1) or 36 h (gel 2) before an inflexion hinted at trace water contamination (Fig. 7). The BMI$^+$PF$_6$$^-$ gel did increase hydrophobicity and, hence, lengthened the time before trace water penetrated onto the lithium surface, as compared with BMI$^+$PF$_6$$^-$ (referring to Figs. 4 and 7). Gel 2 is more hydrophobic due to a higher content of silica (1.5% rather than 1%) than gel 1.

The anode system with gel 3 (BMI$^+$Tf$_2$N$^-$ gel) had decreasing current density with time after 7 h of polarization (Fig. 7). It shows that BMI$^+$Tf$_2$N$^-$ in the gel penetrated onto

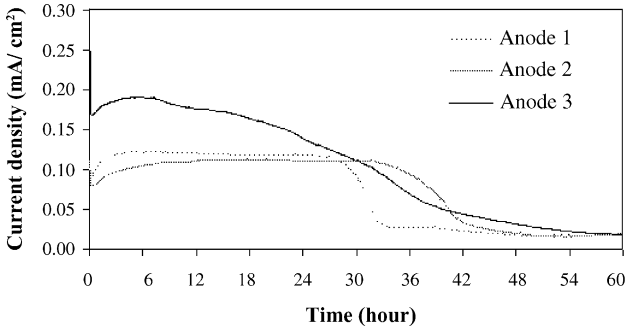

Fig. 7. Polarization current density at +0.5 V overvoltage (vs. OCP) of three lithium anode systems with different silica-gels. *Note*: Anode 1, 2, 3 in the figure respectively represent three lithium anode systems (lithium/BMI$^+$PF$_6$$^-$/Celgard/gel/Celgard) with different gel 1, 2, 3. The ratios of gel 1, 2 and 3 are listed in Table 2.

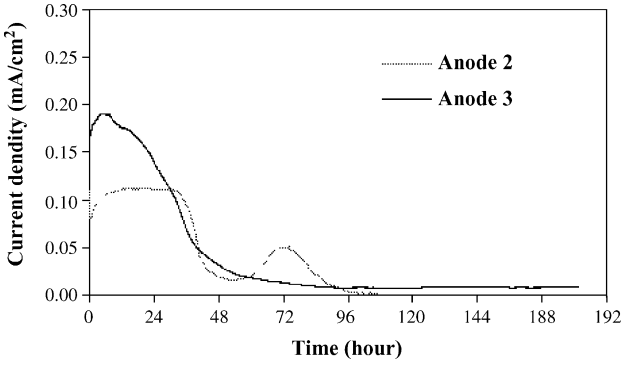

Fig. 8. Polarization current density at +0.5 V overvoltage (vs. OCP) of two lithium anode systems with different silica-gels. *Note*: Anodes 2, 3 in this figure are the same two lithium anode systems as anode 2, 3 in Fig. 7.

the stable lithium/BMI$^+$PF$_6$$^-$ interface after 7 h of operation and had an impact on the current density.

For the lithium anode system with gel 2 (BMI$^+$PF$_6$$^-$ gel) after 60-h polarization, the current density formed a peak (Fig. 8) with concurrent emission of hydrogen gas and formation of LiOH. It shows that trace water penetration accumulated to initiate the reaction Li + H$_2$O → H$_2$ + LiOH when water build-up exceeded a certain concentration (around 1000 ppm [27]). However, the anode system with gel 3 (BMI$^+$Tf$_2$N$^-$ gel) was able to keep a low but constant current density (8 μA cm^{-2}) until we stopped the polarization after 180 h (Fig. 8). No hydrogen gas was observed to evolve and the lithium surface was black lithium–BMI$^+$Tf$_2$N$^-$ interface. Consequently, gel 3 demonstrated higher hydrophobicity than gel 2 and limited water accumulation below the critical concentration initiating the reaction Li + H$_2$O → H$_2$ + LiOH on the lithium–BMI$^+$Tf$_2$N$^-$ interface.

4. Conclusions

The different interactions of lithium metal and ionic liquids resulted in different performances of the lithium/ionic liquid/Celgard anode systems. The non-reactivity of

$BMI^+PF_6^-$ with lithium kept an active lithium surface and enabled the lithium anode system (lithium/$BMI^+PF_6^-$/Celgard) to output constant current density ($\sim$0.2 mA cm^{-2}) with 100% apparent anodic efficiency in 3% NaCl solution under potentiostatic polarization at +0.5 V versus open-circuit potential (OCP). On the contrary, the reactivity of $BMI^+Tf_2N^-$ with lithium formed a porous film on the lithium surface and the lithium anode system (lithium/$BMI^+Tf_2N^-$/Celgard) output decreased the current density (from 0.52 mA cm^{-2} to 0.12 mA cm^{-2}) with 100% apparent anodic efficiency. However, in the above two kinds of lithium anode systems, trace water contamination resulted in the formation of a bilayer film (LiH and LiOH) on the lithium surface and decreased the rate of lithium anodic reaction and hence the discharge current density. $BMI^+Tf_2N^-$performed better than $BMI^+PF_6^-$ for providing a longer time (60 h versus 7 h) before traces of water reached the lithium surface. During the discharge process, both $BMI^+PF_6^-$ and $BMI^+Tf_2N^-$ acted as the stable transport media of Li^+, Cl^-, OH^- and H_2O, but did not react with them because of the excellent chemical stability, high conductivity and high hydrophobicity of these two ionic liquids.

Trace water penetration through the ionic liquids leads to lithium passivity and current density decrease. It has to be avoided or delayed in a lithium anode system for long-term lithium/seawater batteries. $BMI^+PF_6^-$ gel delayed the trace water penetration. Better performance will be expected after minimizing the existing gel porosity and improving the ratios (of silica and PEO to ionic liquid) and the mixing process to get gel with optimum uniformity, viscosity and hydrophobicity. $BMI^+Tf_2N^-$ gel has higher hydrophobicity than $BMI^+PF_6^-$ gel, but its combined usage with $BMI^+PF_6^-$ could not efficiently represent their advantages. $BMI^+Tf_2N^-$ gel alone will be tested further without combining $BMI^+PF_6^-$. On the other hand, if ion-conductive membranes with water blockage can be designed, a lithium/ionic liquid/membrane anode system with high efficiency is not far away from actual application for lithium/seawater batteries.

Acknowledgments

The authors gratefully acknowledge the financial support of this work by Dr. Richard T. Carlin and the Office of Naval Research (Arlington, VA) under Grant No. N00014-99-1-0446, and thank Dr. Jeong-Ju Cho, from LG Chem. Co., Korea, for his assistance in the syntheses of ionic liquids.

References

[1] M.K. Nazeeruddin, A. Kay, J. Rodicio, J. Am. Chem. Soc. 115 (1993) 6382.
[2] N. Papageorgiou, Y. Athanassov, M. Armand, P. Bonhote, J. Electrochem. Soc. 143 (1996) 3099.
[3] J. Fuller, R.T. Carlin, R.A. Osteryoung, J. Electrochem. Soc. 144 (1997) 3881.
[4] V.R. Koch, L.A. Dominey, C. Nanjundiah, M.J. Ondrechen, J. Electrochem. Soc. 143 (3) (1996) 798.
[5] J. Fuller, A.C. Breda, R.T. Carlin, J. Electroanal. Chem. 459 (1998) 29.
[6] C. Nanjundiah, F. McDevit, V.R. Koch, J. Electrochem. Soc. 144 (1997) 3392.
[7] M. Koel, Proc. Estonian Acad. Sci. Chem. 49 (3) (2000) 145.
[8] R. Hagiwara, Y. Ito, J. Fluorine Chem. 105 (2000) 221.
[9] P. Bonhote, A.-P. Dias, N. Papageorgiou, Inorg. Chem. 35 (1996) 1168.
[10] D.R. McFarlane, J. Sun, J.J. Golding, Electrochim. Acta 45 (2000) 1271.
[11] Y. Zhang, M. Urquidi-Macdonald, J. Power Sources 129 (2) (2004) 312.
[12] E.L. Littauer, K.C. Tsai, R.P. Hollandsworth, J. Electrochem. Soc. 125 (1978) 845.
[13] M. Urquidi-Macdonald, D.D. Macdonald, O. Pensado-Rodríguez, J.R. Flores, Electrochim. Acta 47 (2001) 833.
[14] O. Pensado-Rodríguez, J.R. Flores, M. Urquidi-Macdonald, D.D. Macdonald, J. Electrochem. Soc. 146 (4) (1999) 1302.
[15] O. Pensado-Rodríguez, J.R. Flores, M. Urquidi-Macdonald, D.D. Macdonald, J. Electrochem. Soc. 146 (4) (1999) 1326.
[16] Celegard Inc. Website, http://www.celgard.com, last accessed 30 October 2002.
[17] Y. Zhang, Low temperature molten salt membrane lithium/seawater battery. Master thesis. The Pennsylvania State University, 2002.
[18] D. Aurbach, A. Zaban, Y. Ein-Eli, I. Weissman, O. Chusid, B. Markovsky, M. Levi, E. Levi, A. Schechter, E. Granot, J. Power Sources 68 (1997) 91.
[19] D. Aurbach, A. Zaban, Y. Gofer, Y. Ein-Ely, I. Weissman, O. Chusid, O. Abramson, J. Power Sources 54 (1995) 76.
[20] V.R. Koch, C. Nanjundiah, G. Battista Appetecchi, B. Scrosati, J. Electrochem. Soc. 142 (7) (1995) L116.
[21] J.G. Thevenin, R.H. Muller, J. Electrochem. Soc. 134 (11) (1987) 2650.
[22] S. Feliu Jr., R. Barajas, J.M. Bastidas, M. Morcillo, S. Feliu, in: J.R. Scully, D.C. Silverman, M.W. Kendig (Eds.), Electrochemical Impedance: Analysis and Interpretation, ASTM, Philadelphia, PA, 1993, p. 438.
[23] R. Delevie, Electrochemical response of porous and rough surfaces, in: P. Delahay (Ed.), Advances in Electrochemistry and Electrochemical Engineering, 6, 1967, p. 329.
[24] M.W. Kendig, E.M. Meyer, G. Lindberg, F. Mansfeld, Corros. Sci. 23 (1983) 1007.
[25] P.R. Roberge, in: J.R. Scully, D.C. Silverman, M.W. Kendig (Eds.), Electrochemical Impedance: Analysis and Interpretation, ASTM, Philadelphia, PA, 1993, p. 54.
[26] A.K. Jonscher, J. Phys. D: Appl. Phys. 32 (1999) R57–R70.
[27] D. Aurbach, I. Weissman, A. Zaban, P. Dan, Electrochim. Acta 45 (1999) 1135.